The Solid Solution $CeAuIn_{1-x}Mg_x$ – Structure, Magnetic Properties and Specific Heat Data

Sudhindra Rayaprol, Birgit Heying, and Rainer Pöttgen

Institut für Anorganische und Analytische Chemie, Westfälische Wilhelms-Universität Münster, Corrensstraße 30, D-48149 Münster, Germany

Reprint requests to R. Pöttgen. E-mail: pottgen@uni-muenster.de

Z. Naturforsch. **61b,** 495 – 502 (2006); received February 21, 2006

Four different samples of the solid solution $CeAuIn_{1-x}Mg_x$ with $x = 0.2$, 0.4, 0.6, and 0.8 have been prepared from the elements in sealed tantalum tubes in an induction furnace. The samples were characterized through X-ray powder and single crystal data: ZrNiAl type, $P\bar{6}2m$, $Z = 3$, $a = 774.54(7)$, $c = 420.32(10)$ pm, $wR2 = 0.0203$, 395 F^2 values, 15 variables for $CeAuIn_{0.871}Mg_{0.129}$, $a = 775.25(7)$, $c = 419.36(10)$ pm, $wR2 = 0.0488$, BASF $= 0.10(1)$, 397 F^2 values, 16 variables for $CeAuIn_{0.640}Mg_{0.360}$, $a = 774.62(7)$, $c = 420.13(10)$ pm, $wR2 = 0.0435$, 376 F^2 values, 15 variables for $CeAuIn_{0.445}Mg_{0.555}$, $a = 773.80(11)$, $c = 420.82(8)$ pm, $wR2 = 0.0415$, 392 F^2 values, 15 variables for $CeAuIn_{0.228}Mg_{0.772}$. The lattice parameters show no pronounced changes within the solid solution. The largest shift occurs for the x parameter of the mixed occupied In/Mg positions. Due to the difference in size, the trigonal prisms around the Au1 atoms at the origin become smaller with an increasing content of magnesium. The In/Mg–In/Mg distances decrease from 334.5 ($CeAuIn_{0.871}Mg_{0.129}$) to 328.3 ($CeAuIn_{0.228}Mg_{0.772}$) pm, and consequently one observes also shorter bonds to the Au1 atoms with an increasing content of magnesium concentration. Susceptibility measurements reveal trivalent cerium for all $CeAuIn_{1-x}Mg_x$ compounds, with no evidence sign of magnetic ordering down to 2 K. The disorder created by chemical substitution destroys the long-range magnetic ordering which can be attributed to the triggering of non Fermi-liquid (NFL) like behavior.

Key words: Cerium Compounds, Intermetallics, Crystal Chemistry, Magnetism

Introduction

In recent investigations we revealed that the indium and tin atoms in binary transition metal indides and stannides can at least partly be substituted by magnesium [1 – 3, and ref. therein]. These substitutions affect the valence electron concentration of the respective compounds and can have a significant influence on the structure type. For example, the structure type of the solid solution $NiMg_{2-x}Sn_x$ switches from the hexagonal $NiMg_2$ type for small tin concentrations to the orthorhombic $CuMg_2$ type for higher magnesium/tin substitution [3].

The In/Mg and even In/Cd substitution is also possible for ternary compounds, *e. g.* we recently reported on the series *RE*AuMg [4] and *RE*AuCd [5] which are isostructural with the indium compounds, but with a lower electron concentration. The difference in size between indium and magnesium (cadmium) and the change in electron concentration have drastic effects on the properties. To give some examples, in the series EuAuIn [6], EuAuCd [5], and EuAuMg [4, 7], the magnetic ordering temperature increases from 20 K (EuAuIn) to 36 K (EuAuMg). On the other hand, from GdPdIn [8, 9] to GdPdCd [10], the ordering temperature drastically decreases from 102 to 62.5 K.

Besides a full substitution it is also interesting to investigate solid solutions, since different changes in the magnetic ground state can occur. Some interesting examples are the solid solutions $CePt_{1-x}Ni_xSn$ (antiferromagnetic Kondo system ⇔ mixed valence semiconductor transition) [11], $CeRh_{1-x}Ir_xGe$ (antiferromagnetic ⇔ intermediate valence state transition) [12, 13], $URh_{1-x}Ir_xGe$ (antiferromagnetic ⇔ ferromagnetic crossover) [14], or $CeNi_{1-x}T_xSn$ (T = Cu, Pt) (onset of magnetism upon doping) [15].

The non-Fermi liquid (NFL) behavior in transport and thermodynamic properties of rare-earth inter-

Table 1. Lattice parameters of the hexagonal cerium compounds $CeAuIn_{1-x}Mg_x$ with ZrNiAl type structure, space group $P\bar{6}2m$.

Compound	a (pm)	c (pm)	V (nm^3)	Reference
CeAuIn[a]	771	425	0.2188	[18]
CeAuIn[a]	769.8(2)	425.6(1)	0.2184	[21]
$CeAuIn_{0.871}Mg_{0.129}$[b]	774.54(7)	420.32(10)	0.2184	this work
$CeAuIn_{0.8}Mg_{0.2}$[a]	775.0(1)	420.51(5)	0.2187	this work
$CeAuIn_{0.640}Mg_{0.360}$[b]	775.25(7)	419.36(10)	0.2183	this work
$CeAuIn_{0.6}Mg_{0.4}$[a]	776.3(1)	419.87(6)	0.2192	this work
$CeAuIn_{0.445}Mg_{0.555}$[b]	774.62(7)	420.13(10)	0.2183	this work
$CeAuIn_{0.4}Mg_{0.6}$[a]	776.0(1)	420.52(5)	0.2193	this work
$CeAuIn_{0.228}Mg_{0.772}$[b]	773.80(11)	420.82(8)	0.2182	this work
$CeAuIn_{0.2}Mg_{0.8}$[a]	774.8(1)	421.27(7)	0.2190	this work
CeAuMg	774.1(3)	421.6(1)	0.2188	[27]

[a] Powder data; [b] single crystal diffractometer data.

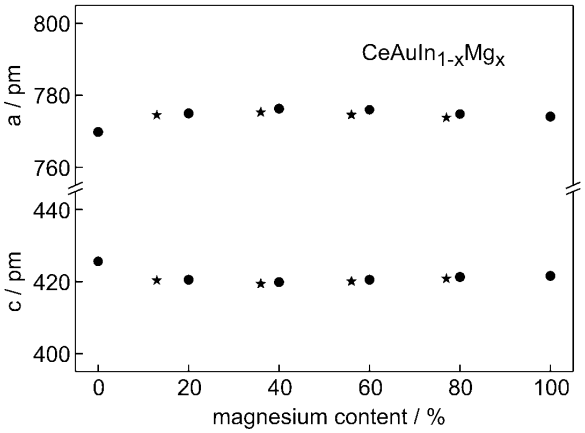

Fig. 1. The course of the cell parameters within the solid solution $CeAuIn_{1-x}Mg_x$ as a function of the magnesium content. Guinier powder and single crystal data are plotted as circles and asterisks, respectively.

metallics (f-electron systems) is a current topic of research in the field of strongly correlated systems. The origin of NFL behavior is currently debated as there are many explanations for the same [16, 17]. Some suggest that the origin of NFL behavior in Ce based Kondo-lattice compounds may also be attributed to the distribution of Kondo temperatures introduced by crystallographic disorder [18]. The NFL behavior is seen in some systems in which f-electron atoms (*RE*) are replaced by nonmagnetic metallic atoms such as $RE_{1-x}M_x$ and also in disordered ligand systems, in which some metal atoms are substituted by a different metal atom such as in $REM_{1-x}M'_x$. Thus, disorder is indeed a very important factor for the occurrence of NFL behavior in these compounds, as is evident from the results of many experiments [16 – 18].

In view of such interesting physical phenomena observed in ternary rare earth intermetallics we have recently started more systematic studies of solid solutions of equiatomic rare earth metal (*RE*)–transition metal (*T*)–indides $RETIn_{1-x}Mg_x$, predominantly with cerium and gadolinium as rare earth metal component. Herein we report on the magnetic behavior of the solid solution $CeAuIn_{1-x}Mg_x$, where the borderline compounds CeAuIn [19 – 26] and CeAuMg [27] show antiferromagnetic ordering at 6 and 2 K, respectively.

Experimental Section

Synthesis

Starting materials for the preparation of the $CeAuIn_{1-x}Mg_x$ samples were sublimed ingots of cerium (Johnson Matthey, > 99.9%), gold foil (Heraeus, > 99.9%), indium tear drops (Johnson-Matthey, > 99.9%), and a magnesium rod (Johnson Matthey, ∅16 mm, > 99.5%; the surface of the rod was first cut on a turning lathe in order to remove surface impurities). In a first step, the cerium ingot was cut into smaller pieces and arc-melted [28] to small buttons (about 500 mg) under an argon pressure of about 600 mbar. The argon was purified before over molecular sieves, silica gel, and titanium sponge (900 K). The cerium buttons were subsequently mixed with the gold foil, pieces of indium and the magnesium rod in the ideal $1:1:1-x:x$ atomic ratios ($x = 0.2,\ 0.4,\ 0.6,\ 0.8$) and sealed in small tantalum tubes under an argon pressure of about 800 mbar.

The tantalum tubes were put in a water-cooled quartz sample chamber of a high-frequency furnace (Hüttinger TIG 5/300) under flowing argon [29]. The tubes were first heated for five minutes at *ca.* 1270 K and subsequently annealed for another four hours at *ca.* 970 K. The temperature was controlled through a Sensor Therm Metis MS09 pyrometer with an accuracy of ±30 K.

The tubes were finally quenched by radiative heat loss within the water-cooled sample chamber. After the annealing procedures the light-grey samples could readily be separated from the tantalum tube. No reactions with the crucible material could be detected. The $CeAuIn_{1-x}Mg_x$ samples are stable in moist air in the form of compact buttons as well as fine-grained powders. Single crystals exhibit metallic lustre.

X-ray film data and structure refinements

The annealed samples were characterized through Guinier powder patterns using Cu-$K_{\alpha 1}$ radiation and α-quartz ($a = 491.30$, $c = 540.46$ pm) as an internal standard. The Guinier camera was equipped with an imaging plate system (Fujifilm BAS–1800). The experimental patterns matched with calculated ones [30] using the atomic positions obtained from the structure refinements. The lattice parameters (Table 1 and

Table 2. Crystal data and structure refinement for $CeAuIn_{0.871(4)}Mg_{0.129(4)}$, $CeAuIn_{0.640(7)}Mg_{0.360(7)}$, $CeAuIn_{0.445(7)}Mg_{0.555(7)}$, and $CeAuIn_{0.228(7)}Mg_{0.772(7)}$, space group $P\bar{6}2m$, $Z = 3$, Pearson symbol hP9.

Empirial formula	$CeAuIn_{0.871}Mg_{0.129}$	$CeAuIn_{0.640}Mg_{0.360}$	$CeAuIn_{0.445}Mg_{0.555}$	$CeAuIn_{0.228}Mg_{0.772}$
Molar mass [g/mol]	440.14	419.02	401.82	382.21
Unit cell dimensions	Table 1	Table 1	Table 1	Table 1
Calculated density [g/cm^3]	10.04	9.56	9.17	8.73
Crystal size [μm^3]	$20\times20\times90$	$10\times40\times60$	$10\times30\times90$	$40\times40\times60$
Transmission (max : min)	1.96	5.65	3.87	2.25
Absorption coefficient [mm^{-1}]	72.2	70.4	69.0	67.4
Detector distance [mm]	–	–	–	60
Exposure time [min]	–	–	–	14
ω Range; increment [°]	–	–	–	$0-180°$; 1.0°
Integr. param. A, B, EMS	–	–	–	13.0; 3.0; 0.014
F(000)	544	518	497	473
θ Range [°]	3 to 35	3 to 35	3 to 35	3 to 35
Range in *hkl*	$\pm12,\pm12,\pm6$	$\pm12,\pm12,\pm6$	$\pm12,\pm12,\pm6$	$\pm11,\pm12,\pm6$
Total no. reflections	3864	3868	3089	3253
Independent reflections	395 ($R_{int} = 0.0509$)	397 ($R_{int} = 0.1233$)	376 ($R_{int} = 0.0803$)	392 ($R_{int} = 0.0400$)
Reflections with $I > 2\sigma(I)$	389 ($R_{sigma} = 0.0210$)	385 ($R_{sigma} = 0.0364$)	367 ($R_{sigma} = 0.0359$)	389 ($R_{sigma} = 0.0179$)
Data / parameters	395 / 15	397 / 16	376 / 15	392 / 15
Goodness-of-fit on F^2	1.197	1.109	1.217	1.069
Final *R* indices [$I > 2\sigma(I)$]	$R1 = 0.0136$	$R1 = 0.0201$	$R1 = 0.0242$	$R1 = 0.0191$
	$wR2 = 0.0201$	$wR2 = 0.0479$	$wR2 = 0.0421$	$wR2 = 0.0415$
R Indices (all data)	$R1 = 0.0145$	$R1 = 0.0220$	$R1 = 0.0262$	$R1 = 0.0194$
	$wR2 = 0.0203$	$wR2 = 0.0488$	$wR2 = 0.0435$	$wR2 = 0.0415$
Flack parameter	$-0.002(6)$	–	$-0.03(1)$	0.00(1)
BASF	–	0.10(1)	–	–
Extinction coefficient	0.0085(3)	0.0079(6)	0.0110(7)	0.0098(6)
Largest diff. peak and hole [e/Å^3]	1.55 and -2.64	3.60 and -3.09	1.79 and -2.03	1.38 and -1.59

Fig. 1) were obtained *via* least-squares fits of the Guinier data.

Irregularly shaped single crystals were isolated from each of the annealed $CeAuIn_{1-x}Mg_x$ samples by mechanical fragmentation and examined by Laue photographs on a Buerger precession camera (equipped with an imaging plate system Fujifilm BAS–1800) in order to establish suitability for intensity data collection. Single crystal intensity data of $CeAuIn_{0.871}Mg_{0.129}$, $CeAuIn_{0.640}Mg_{0.360}$, and $CeAuIn_{0.455}Mg_{0.555}$ were collected at r. t. by use of a four-circle diffractometer (CAD4) with graphite monochromatized Mo-K_α (71.073 pm) radiation and a scintillation counter with pulse height discrimination. The scans were taken in the $\omega/2\theta$ mode and empirical absorptions corrections were applied on the basis of psi-scan data, followed by spherical absorption corrections. Intensity data of $CeAuIn_{0.228}Mg_{0.772}$ were collected at r. t. by use of a Stoe IPDS–II diffractometer with graphite monochromatized Mo-K_α radiation. The absorption correction was numerical. All relevant details concerning the data collections are listed in Table 2.

As expected for ZrNiAl type compounds, space group $P\bar{6}2m$, the four data sets revealed no systematic extinctions. The atomic parameters of CeAuMg [27] were taken as starting values and the structures were refined using SHELXL-97 (full-matrix least-squares on $F_o{}^2$) [31] with anisotropic atomic displacement parameters for all sites. The In/Mg mixing on the 3*g* site was refined as a least squares variable. All other sites were fully occupied within two standard uncertainties. Refinement of the correct absolute structure was ensured through refinement of the Flack parameter [32, 33]. Only the $CeAuIn_{0.640}Mg_{0.360}$ crystal revealed twinning by inversion. Final difference Fourier syntheses revealed no significant residual peaks (see Table 2). The highest residual densities were close to the cerium positions and most likely resulted from incomplete absorption corrections of these strongly absorbing intermetallics. The refined positional parameters and interatomic distances are listed in Tables 3 and 4. Further details on the structure refinements are available*.

EDX analyses

The bulk samples and the single crystals measured on the diffractometers were analyzed by EDX using a LEICA 420 I scanning electron microscope with CeO_2, Au, InAs, and MgO as standards. The single crystals mounted on the

*Details may be obtained from: Fachinformationszentrum Karlsruhe, D-76344 Eggenstein-Leopoldshafen (Germany), by quoting the Registry No's. CSD–416269 ($CeAuIn_{0.871}Mg_{0.129}$), CSD–416270 ($CeAuIn_{0.640}Mg_{0.360}$), CSD–416271 ($CeAuIn_{0.445}Mg_{0.555}$), and CSD–416272 ($CeAuIn_{0.228}Mg_{0.772}$).

Atom	Wyckoff site	occupancy/ %	*x*	*y*	*z*	U_{eq}
$CeAuIn_{0.871(4)}Mg_{0.129(4)}$						
Ce	3*f*	100	0.58699(5)	0	0	69(1)
Au1	1*a*	100	0	0	0	84(1)
Au2	2*d*	100	1/3	2/3	1/2	82(1)
In/Mg	3*g*	87.1(4)/12.9(4)	0.24933(6)	0	1/2	79(2)
$CeAuIn_{0.640(7)}Mg_{0.360(7)}$						
Ce	3*f*	100	0.58689(9)	0	0	86(2)
Au1	1*a*	100	0	0	0	101(2)
Au2	2*d*	100	1/3	2/3	1/2	97(1)
In/Mg	3*g*	64.0(7)/36.0(7)	0.24849(15)	0	1/2	90(4)
$CeAuIn_{0.445(7)}Mg_{0.555(7)}$						
Ce	3*f*	100	0.58633(10)	0	0	100(2)
Au1	1*a*	100	0	0	0	118(2)
Au2	2*d*	100	1/3	2/3	1/2	111(2)
In/Mg	3*g*	44.5(7)/55.5(7)	0.2468(2)	0	1/2	109(5)
$CeAuIn_{0.228(7)}Mg_{0.772(7)}$						
Ce	3*f*	100	0.41426(9)	0	0	122(1)
Au1	1*a*	100	0	0	0	138(1)
Au2	2*d*	100	2/3	1/3	1/2	131(1)
In/Mg	3*g*	22.8(7)/77.2(7)	0.7551(3)	0	1/2	116(7)

Table 3. Atomic coordinates and isotropic displacement parameters for $CeAuIn_{0.871(4)}Mg_{0.129(4)}$, $CeAuIn_{0.640(7)}Mg_{0.360(7)}$, $CeAuIn_{0.445(7)}Mg_{0.555(7)}$, and $CeAuIn_{0.228(7)}Mg_{0.772(7)}$, space group $P\bar{6}2m$. U_{eq} (pm^2) is defined as one third of the trace of the orthogonalized U_{ij} tensor.

			$In_{0.871}Mg_{0.129}$	**$In_{0.640}Mg_{0.360}$**	**$In_{0.445}Mg_{0.555}$**	**$In_{0.228}Mg_{0.772}$**	**$Mg_{1.00}$**
Ce:	4	Au2	314.2	314.0	314.0	314.0	314.2
	1	Au1	319.9	320.3	320.4	320.6	321.2
	2	*M*	335.5	335.9	336.6	337.4	339.7
	4	*M*	349.3	349.2	349.4	349.6	350.0
	4	Ce	404.5	404.8	404.3	403.6	403.5
	2	Ce	420.3	419.4	420.1	420.8	421.6
Au1:	6	*M*	285.4	284.7	284.0	283.2	281.5
	3	Ce	319.9	320.3	320.4	320.6	321.2
Au2:	3	*M*	296.1	296.8	297.5	298.1	300.2
	6	Ce	314.2	314.0	314.0	314.0	314.2
M:	2	Au1	285.4	284.7	284.0	283.2	281.5
	2	Au2	296.1	296.8	297.5	298.1	300.2
	2	*M*	334.5	333.7	331.1	328.3	323.1
	2	Ce	335.5	335.9	336.6	337.4	339.7
	4	Ce	349.3	349.2	349.4	349.6	350.0

Table 4. Interatomic distances (pm) in the structures of $CeAuIn_{0.871}Mg_{0.129}$, $CeAuIn_{0.640}Mg_{0.360}$, $CeAuIn_{0.445}Mg_{0.555}$, and $CeAuIn_{0.228}Mg_{0.772}$. Standard deviations are equal or less than 0.4 pm. All distances within the first coordinate spheres are listed. *M* denotes the In/Mg mixing on the 3*g* site (see Table 3). The data for CeAuMg [24] are listed for comparison.

quartz fibers were coated with a thin carbon film. Pieces of the bulk samples were polished with different silica and diamond pastes and left unetched for the analyses in the scanning electron microscope in backscattering mode. The EDX analyses revealed no impurity elements and were in agreement with the refined compositions.

Physical property measurements

The samples of the series $CeAuIn_{1-x}Mg_x$ were packed in gelatin capsules and attached to the sample holder rod of the ACMS for measuring magnetic properties in a Quantum Design Physical-Property-Measurement-System in the temperature range 2 – 300 K with magnetic flux densities up to 80 kOe. For heat capacity (C_p) measurements the samples were glued to the platform of the pre-calibrated heat capacity puck using *Apizeon N grease*.

Discussion

Crystal chemistry

The intermetallic compounds within the solid solution $CeAuIn_{1-x}Mg_x$ crystallize with the hexagonal ZrNiAl type structure, similar to the borderline compounds CeAuIn [19] and CeAuMg [27]. The lattice parameters (Fig. 1) show no pronounced changes over the whole solid solution. A small discrepancy occurs between the refined compositions of the single crystals and the starting compositions of the samples. Systematically, the crystals have a slightly smaller magnesium content. This is indicative of small inhomogeneities in the samples.

A projection of the $CeAuIn_{1-x}Mg_x$ structure is presented in Fig. 2. The two crystallographically indepen-

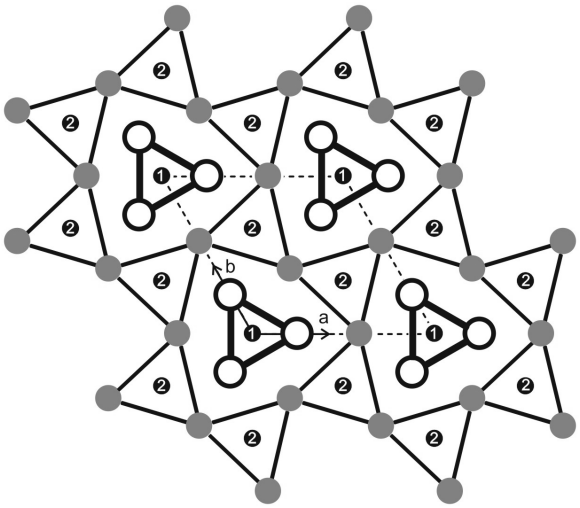

Fig. 2. Projection of the $CeAuIn_{1-x}Mg_x$ structure onto the *xy* plane. All atoms lie on mirror planes at $z = 0$ (thin lines) and $z = 1/2$ (thick lines). Cerium, gold, and indium/magnesium atoms are drawn as medium grey, black filled, and open circles, respectively. The trigonal prismatic units and the two crystallographically independent gold sites are emphasized.

dent gold sites fill the trigonal prisms built up from the cerium and In(Mg) atoms. The two prismatic motifs are shifted with respect to each other *via* half the translation period *c*. The crystal chemistry and chemical bonding in various ZrNiAl related materials have repeatedly been discussed in literature [34 – 36]. For details we refer to these articles. Herein we focus only on the peculiarities of the solid solution.

The largest shift within the solid solution occurs for the *x* parameter of the 3*g* In/Mg site: from $x = 0.24933$ for $CeAuIn_{0.871}Mg_{0.129}$ to $x = 0.2410$ for CeAuMg. This shift is directly related to the different sizes of indium and magnesium which have covalent radii of 150 and 136 pm [37], respectively. With increasing magnesium content the trigonal prism around the Au1 atoms (origin of the cell) becomes smaller. Consequently we also observe shorter In/Mg–In/Mg (334.5 → 323.1 pm) and Au1–In/Mg (285.4 → 281.5 pm) distances with increasing magnesium content. On the other hand the Ce–In/Mg (335.5 → 339.7 pm) and Au2–In/Mg (296.1 → 300.2 pm) distances increase (Table 4).

Due to the statistical occupancy of the 3*g* site by indium and magnesium, the cerium atoms have a varying coordination, and these inhomogeneities may account for the destruction of magnetic long-range ordering *vide infra*.

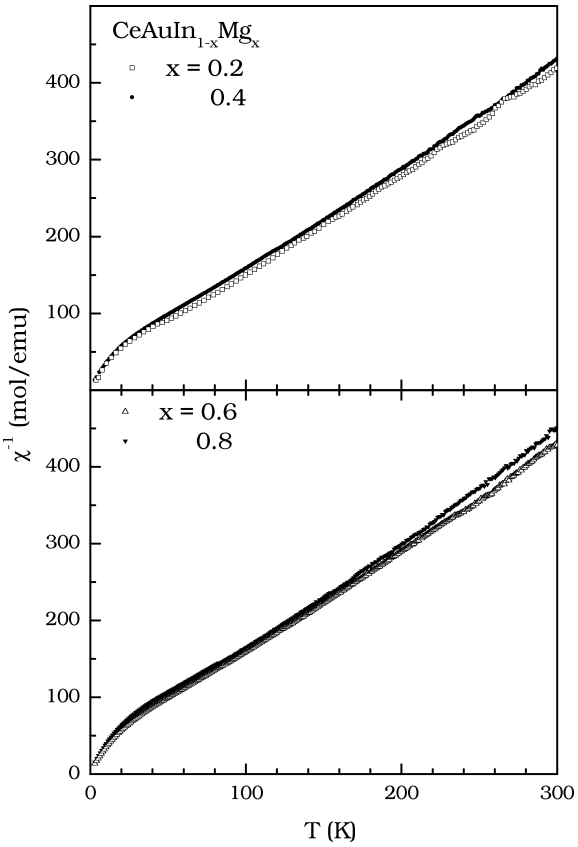

Fig. 3. Inverse susceptibility of $CeAuIn_{1-x}Mg_x$ measured under a steady applied field of 10 kOe.

Magnetic properties and specific heat data

In Fig. 3, we show the inverse susceptibility (χ^{-1}) for all samples of the $CeAuIn_{1-x}Mg_x$ series measured after zero field cooling from r. t. in each case. A steady field of 10 kOe was applied for measuring the susceptibility of the $x = 0.2 - 0.6$, and of 5 kOe for the $x = 0.8$ samples. It can be clearly seen that the partial substitution of magnesium for indium destroys the long-range magnetic ordering observed in the end members, namely, CeAuIn ($T_N = 6$ K) [23, 38] and CeAuMg (2 K) [27]. Even for the higher concentrations of indium we could not detect any magnetic ordering up to the lowest temperature measured (2 K). The susceptibility (χ) follows Curie-Weiss law above 100 K. From the linear region of χ^{-1} *vs.* T plots, we have calculated the paramagnetic Curie temperature (θ_p) and the effective Bohr magneton number (μ_{eff}) for each sample (Table 5). With varying In/Mg concentration, θ_p changes marginally and remains negative indicating antiferro-

Table 5. Values of paramagnetic Curie temperature (θ_p), Bohr magneton number (μ_{exp}), and electronic specific heat coefficient (γ) for the series $CeAuIn_{1-x}Mg_x$.

Sample	θ_p (K)	μ_{exp} (μ_B/Ce atom)	γ (mJ/mol K^2)	Reference
CeAuIn	−10	2.50	30	[23]
$CeAuIn_{0.8}Mg_{0.2}$	−12.6(2)	2.46(3)	157(5)	this work
$CeAuIn_{0.6}Mg_{0.4}$	−11.4(2)	2.42(3)	10(3)	this work
$CeAuIn_{0.4}Mg_{0.6}$	−16.9(2)	2.44(3)	10(3)	this work
$CeAuIn_{0.2}Mg_{0.8}$	−9.4(2)	2.36(3)	71(3)	this work
CeAuMg	−57(1)	2.6(1)	9*	[27]

* The value of γ estimated from the non-magnetic isostructural compound LaAuMg.

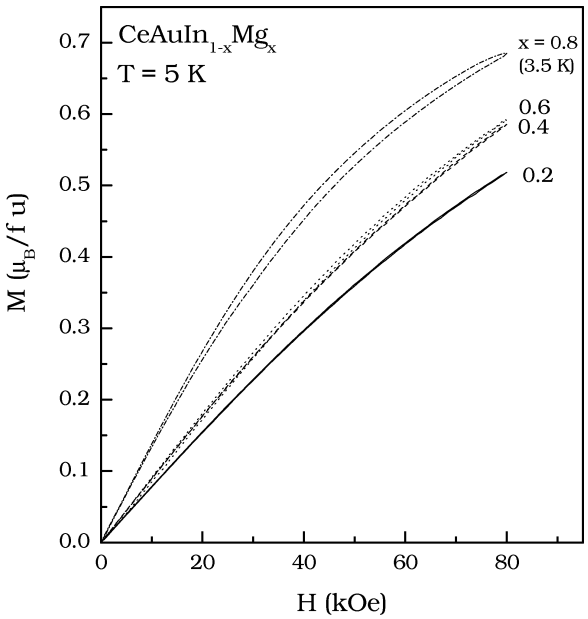

Fig. 4. Isothermal magnetization for $CeAuIn_{1-x}Mg_x$ measured at 5 K (3.5 K for x = 0.8).

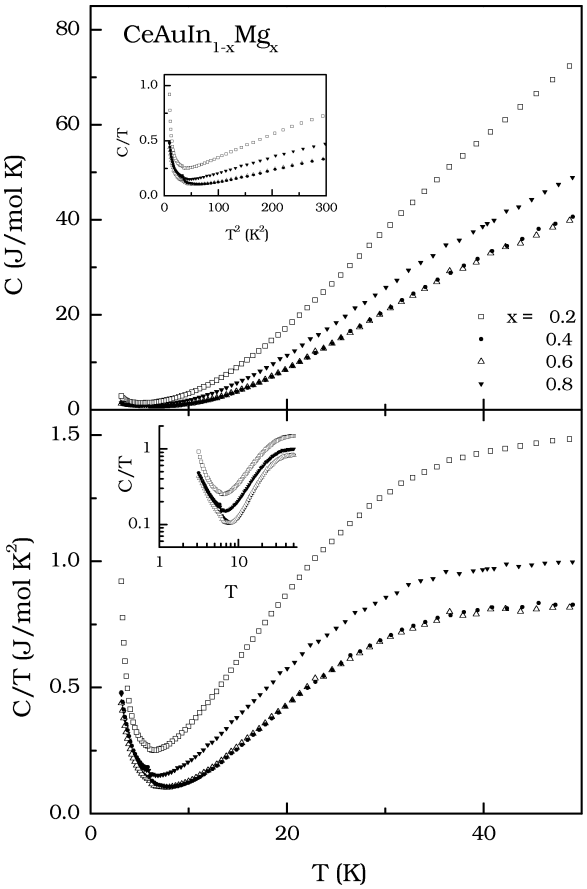

Fig. 5. Specific heat of $CeAuIn_{1-x}Mg_x$ plotted in several ways. C/T *vs.* T^2 is plotted as insert to highlight the linear region. In another insert, C/T *vs.* T is plotted on a log-log scale, to show the almost linear variation of C/T at low temperatures.

magnetic interactions persisting up to high temperatures. The magnetic moment of the cerium atoms is marginally affected by the In/Mg mixing and the values are slightly less than the expected value of 2.54 μ_B for a free Ce^{3+} ion. Comparing the values of θ_p and μ_{eff} of the series $CeAuIn_{1-x}Mg_x$ with the end members (Table 5), it is clear that the intermixing of ions has affected these quantities marginally, but the magnetic interactions are predominantly antiferromagnetic in the entire range.

It may be recalled that for the series of *RE*AuIn compounds with ZrNiAl type structure, the explanation for the magnetic ordering has been attributed to RKKY interactions owing to the large *RE–RE* interatomic distances of about 400 pm [26]. However for the solid-solution of $CeAuIn_{1-x}Mg_x$, the magnetic long-range ordering is lost because of chemical substitution. The In/Mg mixing does not affect the structure, as there is only a marginal change in lattice parameters (crystal structure), it however strongly affects the long range ordering of the cerium magnetic moments. In order to ascertain the magnetic behavior of this series, we have measured the isothermal magnetization (M–H curves) at low temperatures up to a field strength of 80 kOe. In Fig. 4, we show the M(H) loops for the whole series. The magnetization exhibits a typical antiferromagnetic state for all samples, but does not saturate even up to 80 kOe, indicating complex ordering patterns of spin canting as observed in the end members also [27]. The reduction in the saturation moment accompanied by the loss of magnetic ordering (in the measured tem-

perature range) can also be caused by the averaging effects of the polycrystalline sample, or by an influence of crystal field or hybridization effects (*e. g.*, Kondo effect). The M(H) also clearly establishes that increasing Mg content increases the disorder in the system, presumably due to the change in the electron count, resulting in further lowering of the moment values.

The complex magnetic behavior of this solid solution can be further observed also from the specific heat measurements. We have measured the specific heat (C) of all compounds of the $CeAuIn_{1-x}Mg_x$ series to 3 K. In Fig. 5, we show the heat capacity plotted in different forms. No magnetic ordering could be seen in the C(T) curves also. However the plot of C/T *vs.* T is quite interesting. For all compounds, below 10 K, the plot of C/T *vs.* T, varies logarithmically (almost linearly when plotted on log-log scale, insert in Fig. 5) indicating NFL like characteristics [15 – 18]. Owing to the upturn in the plot of C/T *vs.* T^2 at lower temperatures, the electronic specific heat capacity coefficient (γ) has been calculated for a higher temperature range $(100 < T^2 < 300)$. The values of γ calculated for all samples in the series are listed in Table 5. It should be noted here that these γ values also contain the contribution from the lattice part, as we have not subtracted the lattice contribution to the total heat capacity.

Finally, we observe that chemical disorder created by In/Mg mixing results in the destruction of long-range magnetic ordering and may also be responsible for the observation of NFL like characteristics in the $CeAuIn_{1-x}Mg_x$ series. It is interesting to note that chemical substitution has not changed the structure as much as it has changed the magnetic nature of these compounds. Small mixing of In/Mg is enough to destroy the long-range ordering, which can be partially attributed to both crystallographic and electronic effects. We believe that more detailed measurements to lowest temperatures are needed to understand the nature of magnetism in these compounds.

Acknowledgements

We thank H.-J. Göcke for the work at the scanning electron microscope and Dipl.-Ing. U. Ch. Rodewald for help with the intensity data collections. This work was supported by the Deutsche Forschungsgemeinschaft. S.R. is indebted to the Alexander von Humboldt-Stiftung for a research grant.

[1] M. Schlüter, U. Häussermann, B. Heying, R. Pöttgen, J. Solid State Chem. **173**, 418 (2003).
[2] V. Hlukhyy, R. Pöttgen, J. Solid State Chem. **178**, 79 (2005).
[3] V. Hlukhyy, U. Ch. Rodewald, R. Pöttgen, Z. Anorg. Allg. Chem. **631**, 2997 (2005).
[4] R. Pöttgen, R.-D. Hoffmann, J. Renger, U. Ch. Rodewald, M. H. Möller, Z. Anorg. Allg. Chem. **626**, 2257 (2000).
[5] R. Mishra, R. Pöttgen, R.-D. Hoffmann, D. Kaczorowski, H. Piotrowski, P. Mayer, C. Rosenhahn, B. D. Mosel, Z. Anorg. Allg. Chem. **627**, 1283 (2001).
[6] R. Pöttgen, J. Mater. Chem. **6**, 63 (1996).
[7] D. Johrendt, G. Kotzyba, H. Trill, B. D. Mosel, H. Eckert, Th. Fickenscher, R. Pöttgen, J. Solid State Chem. **164**, 201 (2002).
[8] K. H. J. Buschow, J. Less-Common Met. **39**, 185 (1975).
[9] J. W. C. de Vries, R. C. Thiel, K. H. J. Buschow, J. Less-Common Met. **111**, 313 (1985).
[10] R.-D. Hoffmann, Th. Fickenscher, R. Pöttgen, C. Felser, K. Łątka, R. Kmieć, Solid State Sci. **4**, 609 (2002).
[11] J. Sakurai, R. Kawamura, T. Taniguchi, S. Nishigori, S. Ikeda, H. Goshima, T. Suzuki, T. Fujita, J. Magn. Magn. Mater. **104 – 107**, 1415 (1992).
[12] B. Chevalier, P. Rogl, E. K. Hlil, M. H. Tuilier, P. Dordor, J. Etourneau, Z. Phys. Chem. B: Condens. Matter **84**, 205 (1991).
[13] E. Gaudin, B. Chevalier, B. Heying, U. Ch. Rodewald, R. Pöttgen, Chem. Mater. **17**, 2693 (2005).
[14] B. Chevalier, E. Hickey, J. Etourneau, J. Magn. Magn. Mater. **90 – 91**, 499 (1990).
[15] G. M. Kalvius, A. Kratzer, G. Grosse, D. R. Noakes, R. Wäppling, H. v. Löhneysen, T. Takabatake, Y. Echizen, Physica B **289 – 290**, 256 (2000).
[16] T. Graf, J. D. Thompson, M. F. Hundley, R. Movshovich, Z. Fisk, D. Mandrus, R. A. Fisher, N. E. Philips, Phys. Rev. Lett. **78**, 3769 (1997).
[17] A. H. Castro Neto, G. Castilla, B. A. Jones, Phys. Rev. Lett. **81**, 3531 (1998).
[18] O. O. Bernal, D. E. MacLaughlin, H. G. Lukefar, B. Andraka, Phys. Rev. Lett. **75**, 2023 (1995).
[19] A. E. Dwight, Proc. Rare Earth Res. Conf. **1**, 480 (1976).
[20] R. Marazza, R. Ferro, V. Contardi, D. Mazzone, G. Rambaldi, D. Rossi, G. Zanicchi, Proc. Rare Earth Res. Conf. **1**, 308 (1976).
[21] D. Rossi, R. Ferro, V. Contardi, R. Marazza, Z. Metallkd. **68**, 493 (1977).
[22] K. R. Bauchspiess, W. Boksch, E. Holland-Moritz, H. Launois, R. Pott, D. Wohlleben, Valence Fluctua-

tions in Solids, p. 417, St. Barbara Inst. Theor. Phys. Conf., North-Holland, Amsterdam (1981).
[23] H. R. Pleger, E. Bruck, E. Braun, F. Oster, A. Freimuth, B. Politt, B. Roden, D. Wohlleben, J. Magn. Magn. Mater. **63&64**, 107 (1987).
[24] Ł. Gondek, A. Szytuła, B. Penc, J. M. Hernandez-Velasco, A. Zygmunt, J. Magn. Magn. Mater. **262**, L177 (2003).
[25] Ł. Gondek, A. Szytuła, S. Baran, J. M. Hernandez-Velasco, J. Magn. Magn. Mater. **272 – 276**, e443 (2004).
[26] A. Szytuła, Ł. Gondek, B. Penc, J. M. Hernandez-Velasco, Acta Phys. Polon. A **106**, 583 (2004).
[27] B. J. Gibson, A. Das, R. K. Kremer, R.-D. Hoffmann, R. Pöttgen, J. Phys.: Condens. Matter **14**, 5173 (2002).
[28] R. Pöttgen, Th. Gulden, A. Simon, GIT Labor Fachzeitschrift **43**, 133 (1999).
[29] D. Kußmann, R.-D. Hoffmann, R. Pöttgen, Z. Anorg. Allg. Chem. **624**, 1727 (1998).
[30] K. Yvon, W. Jeitschko, E. Parthé, J. Appl. Crystallogr. **10**, 73 (1977).
[31] G. M. Sheldrick, SHELXL-97, Program for Crystal Structure Refinement, University of Göttingen, Germany (1997).
[32] H. D. Flack, G. Bernadinelli, Acta Crystallogr. A **55**, 908 (1999).
[33] H. D. Flack, G. Bernadinelli, J. Appl. Crystallogr. **33**, 1143 (2000).
[34] E. Parthé, L. Gelato, B. Chabot, M. Penzo, K. Cenzual, R. Gladyshevskii, TYPIX – Standardized data and crystal chemical characterization of inorganic structure types. Gmelin Handbook of inorganic and organometallic chemistry, 8th edition, Springer, Berlin (1993).
[35] M. F. Zumdick, R. Pöttgen, Z. Kristallogr. **214**, 90 (1999).
[36] M. F. Zumdick, R.-D. Hoffmann, R. Pöttgen, Z. Naturforsch. **54b**, 45 (1999).
[37] J. Emsley, The Elements, Oxford University Press, 3rd ed. (1999).
[38] Ł. Gondek, B. Penc, A. Szytuła, A. Jezierski, A. Zygmunt, Acta Phys. Polon. B **34**, 1209 (2003).